Nonlinear Dyn (2024) 112:21729–21750
https://doi.org/10.1007/s11071-024-10175-z

RESEARCH

Nonlinear mathematical modeling of frequency-temperature dependent viscoelastic materials for tire applications

Aleksandr Sakhnevych · Raffaele Maglione · Raffaele Suero · Lina Mallozzi

Received: 18 April 2024 / Accepted: 13 August 2024 / Published online: 4 September 2024

Abstract Understanding and accurately reproducing the realistic response of rubber materials to external stimuli is a crucial research topic that involves all the engineering fields and beyond where these materials are used. This study introduces an innovative nonlinear fractional derivative generalized Maxwell model designed to effectively capture and replicate the experimental behavior of viscoelastic materials. The proposed model addresses the limitations observed in conventional fractional models, providing greater versatility which makes it more suitable for describing the intricate behavior of polymeric materials. Through rigorous mathematical validation, the proposed model demonstrates coherence with the underlying physics of the viscoelastic behavior. To address the identification procedure, the pole-zero formulation is adopted, employing a multi-objective optimization to obtain the optimum, able to replicate the dynamic moduli trends. Satisfying results have been validated over a wide dataset of 10 different materials, demonstrating an extended capability of adapting to different variations than classical widely-used fractional models. Furthermore, the model has proven to be valid even employing a reduced amount of experimental data limited only to low, high-frequency plateaus and around the glass transition temperature, which could be fundamental for optimizing resources in experimental investigations.

Keywords Polymers · Viscoelastic modeling · Fractional derivative approach · Material characterization · Analytical demonstration · Nonlinear modeling

A. Sakhnevych · R. Maglione · R. Suero (✉)
Department of Industrial Engineering, University of Naples Federico II, 80125 Naples, Italy
e-mail: raffaele.suero@unina.it

A. Sakhnevych
e-mail: aleksandr.sakhnevych@unina.it

R. Maglione
e-mail: raffaele.maglione@unina.it

L. Mallozzi
Member of GNAMPA-INDAM, 00185 Rome, Italy
e-mail: lina.mallozzi@unina.it
Department of Mathematics and Applications, University of Naples Federico II, 80125 Naples, Italy

1 Introduction

Viscoelastic materials, characterized by their distinctive combination of viscous and elastic properties under mechanical stresses, have become integral components across a wide spectrum of applications due to their versatile nature. Besides the biomedical field [1,2], in civil applications [3] and for aerospace structures and industrial machinery [4–6], these materials assume relevant importance also in the mobility sector, since especially the tires, representing the only interface between vehicles and roads, strongly influence vehicles' handling, safety, fuel efficiency, and environmental impact criteria [7,8].

The dynamic behavior of structures that use rubber materials can be especially valuable to know both in

the early stages of product design and during its use and aging. A reliable model can help with simulation analysis and predicting how a product with a specific material will act in certain solicitation and temperature conditions, considering both geometric and structural characteristics [9]. A proper physical and mathematical model can be fundamental to conducting accurate Finite Element Analysis (FEA) and Complex Eigenvalues Analysis (CEA) for structures with polymeric elements, where a purely elastic model can become insufficient [10,11]. Furthermore, realistic models of materials can be employed to monitor the behavior of existing products throughout their whole life cycle and make reliable forecasts of their performance taking into account their mutuating performance due to aging or other factors.

In this context, an ongoing challenge that this study aims at proposing concerns the optimal mathematical formulation for the representation of the viscoelastic material's behavior, relying on a reduced number of model parameters which can be calibrated on a limited number of data samples, in a frequency (or temperature) range, more or less restricted partial data, depending on the testing equipment employed for the acquisition.

The experimental data represent the basis for developing these viscoelastic materials models which could prove very useful and essential in different applications. The characterization of rubber materials can be conducted in different ways: static tests, making use of static or quasi-static application of loads or deformations, and non-stationary tests which can be classified according to whether they are conducted in the time or frequency domain [12]. Specifically, time-based procedures are also known as transient testing because they involve the application of a deformation or load (elongation or shear) to the material that varies over time and the analysis of its response. These include impact tests, creep experiments, and stress-relaxation experiments. Frequency-based procedure are usually referred to as dynamic tests and include techniques such as the Dynamic Mechanical Analysis (DMA) [13], which involves soliciting the material sample with frequency-varying stress or strain and measuring the magnitude and phase of the resulting frequency response to define intrinsic characteristics moduli. These methodologies are usually destructive, but innovative tools capable of non-destructive conducting fast and accurate dynamic testing of polymeric materials in a non-invasive way are also emerging, such as the VESevo device able to evaluate in a non-destructive way the viscoelastic characteristics of a finished product (i.e. tires), by studying the dynamics of a free bouncing rod [14].

From a mathematical point of view, the most common approach to defining a viscoelastic constitutive law consists of using linear differential models based on Boltzmann's superposition principle [15], which provides an integral representation of linear viscoelasticity, that represents an alternative to the differential form [16]. The linear models are a combination of two kinds of mechanical elements, a perfect elastic spring, describing the elastic part of the viscoelastic behavior, and a perfect viscous dashpot, which reproduces the hysteretic response. The stress and the strain are linked through linear differential equations whose complexity depends on the number of elements. Basic models, like the Maxwell or the Kelvin–Voigt (KV), are described by simple equations, but they fail at representing creep and relaxation phenomena, respectively, even though they remain locally efficient within small frequency ranges. To overcome these limits and to formulate an approach capable of describing the viscoelastic behavior in a wide range of frequencies and time scales, combinations of Maxwell or KV elements, in series or parallel, can be used, obtaining the generalized Maxwell or KV models [17]. However, the complex constitutive equations of these approaches make use of a large set of parameters, which are hard to determine, making their use impractical. For this reason, an alternative representation of polymeric materials is gaining prominence in various applications, namely the fractional models, which, by replacing the dashpots with new elements, the spring-pots, allow a more accurate representation of the viscoelastic behavior with a reduced number of parameters, even in a wider range of excitation frequencies [18].

The introduction of fractional elements to accurately reconstruct the rheological behavior of rubber materials is a very widespread research topic in the literature in numerous fields of application [19–23]. In the context of the mechanics of solids, many dynamic problems have been studied making use of fractional calculus, as described in the detailed review by Shitikova [24]. In [25] the authors demonstrate that fractional derivative models perform better than than integer order ones in reproducing the behavior of biological tissues. Use in the food sector is also common, comprehending liquid food solutions [26], food gels [27], and food

additives [28]. Other studies demonstrate the ability of the fractional model to reproduce the dynamic moduli trend of magnetorheological elastomers with frequency [29,30].

However, no unique methodology exists to identify the optimal set of model parameters to adequately reproduce viscoelastic behavior; indeed, the calibration procedures range from genetic algorithm methods [31,32], to curve fitting methods [33,34] or numerical optimization techniques [35,36]. Furthermore, these models are often validated in specific simulation environments on ideal materials or towards experimental data limited in a narrow frequency range. Contrary to the above limitations, this work aims to verify the robustness of the results employing experimental data acquired through the DMA technique available over a vast range of frequencies. In particular, following the approach introduced by Renaud et al. in [37] and also used by Genovese et al. in [38], the pole-zero formulation, in the case of the GM model, has been employed, considerably reducing the computation complexity of the calibration procedure. The limit of the above models, however, regards its intrinsic linearity which does not always allow an adequate description of the viscoelastic behavior of materials, especially when the exciting stress becomes more significant or the solicitation frequencies are higher. Different sources determine a non-linear response of polymers, including aging, strain softening, and annealing, which have been taken into account in some studies through non-linear elements (masses or dashpots) [39,40]. Jrad et al. in [41] studied a generalized Maxwell model with a non-linear spring and a predetermined number of linear Maxwell cells proving its ability to accurately reproduce the modulus and phase of the complex viscoelastic modulus, albeit in a narrow frequency range.

This work proposes an improved formulation for the mathematical description of the viscoelastic materials' behavior making use of the existing fractional models with an addition consisting of an isolated elastic element with a frequency-varying stiffness, validating the results over an extensive set of materials. This model demonstrates an improved description of the viscoelastic properties at both low and high frequencies and over an extensive time scale, which was a common problem with the conventional linear models, especially for the storage modulus curves, as can be seen in an example of application in Fig. 1 for a compound demonstrating a considerable variability at low frequencies with a marked double slope in the viscoelastic region, as can be seen around 10^7 rad/s frequency.

Another common problem, common in the calibration of fractional models and addressed by the authors regards the definition of a multi-objective optimization routine, able to guarantee the desired approximation tolerances towards both storage modulus E' and loss factor $\tan\delta$, which becomes absolutely non-trivial in case of significant nonlinear variations, especially at low frequencies. Finally, additional research has been done to determine the minimum quantity of experimental data depending on the frequency ranges covered, which is required to accurately and fairly reproduce the viscoelastic behavior of the materials over the necessary frequency or temperature range.

The paper is organized as follows: in Sect. 2, a description of the viscoelastic material models adopted is reported, introducing the fractional calculus and the frequency-domain definition of these models in the pole-zero formulation. In Sect. 3 the model parameters identification algorithm is presented, defining and validating from a mathematical point of view the introduction of a non-linear element, necessary to improve the performance of the presented model. Sect. 4, following a light digression on the materials' characteristics and experimental equipment, present the results and discussions of the model's application on data covering the entire experimentally tested frequency range and only a portion of it, while Sect. 5 contains the conclusion and future developments.

2 Physical endeavor and mathematical framework

In this chapter, following a brief introduction to the rheological behavior of viscoelastic materials and their dependence on frequency and temperature, the design of a novel mathematical formulation is discussed using a fractional derivative framework. In particular, a specific poles and zeros based transformation is recalled which according to recent studies has shown remarkable robustness in its results [37,38], although it presents limitations that will be explored and described for the sake of completeness in the next chapter.

2.1 Viscoelastic material's behavior

The response of viscoelastic materials results from a combination of elastic and viscous behavior under external stimuli. When this class of materials is

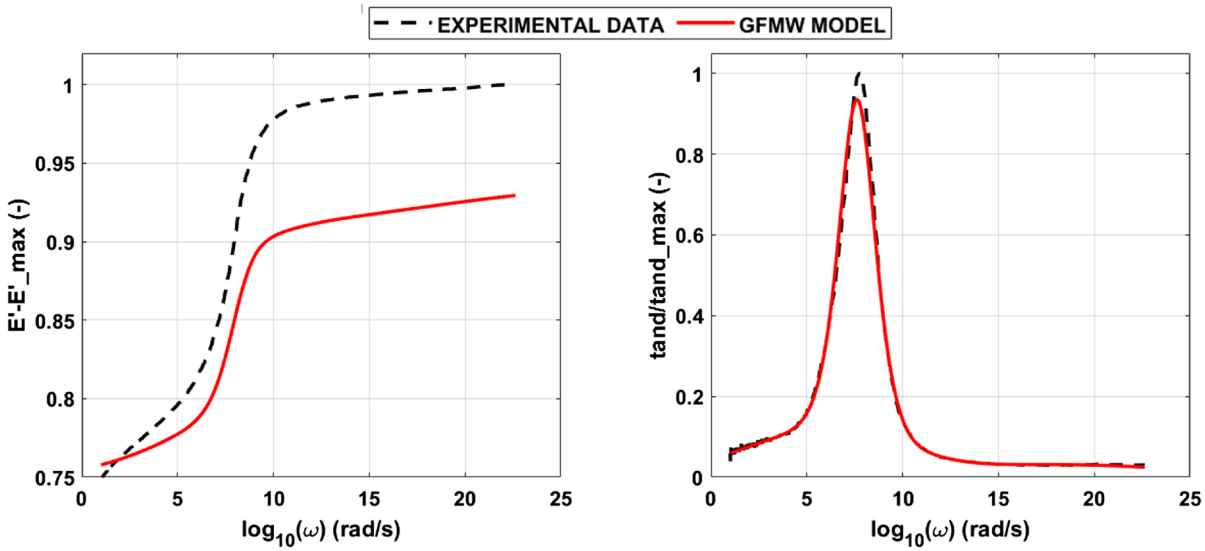

Fig. 1 Example of approximation of viscoelastic proprieties (storage modulus E' on the left and loss factor $\tan\delta$ on the right) for a generic tire compound fitted a Generalized Fractional Maxwell Model (GFMW)

solicited, their response can be divided into an instantaneous reaction, generated by the changing molecular distance, followed by a consequent deformation, as a result of the reorganization of polymeric chains.

Specifically, if sinusoidal stress, characterized by an amplitude σ_0 and angular frequency $\omega = 2\pi f$, is applied on a viscoelastic material, it determines a microscopic reorganization which results in a sinusoidal strain with an amplitude ε_0 at the same frequency of the input stress but with a phase lag δ, linked to the energy dissipation inside the material. From a macroscopic point of view, it is possible to underline the double nature of elements by normalizing the two responses according to the amplitude of solicitation σ_0, obtaining the storage modulus E' (Pa) and the loss modulus E'' (Pa), which compose the dynamic stiffness E^* and define the phase lag δ according to Eqs. (1 and 2), respectively.

$$\frac{\sigma(\omega)}{\varepsilon(\omega)} = E^* = E' + jE'' \tag{1}$$

$$tan(\delta) = \frac{E''}{E'} \tag{2}$$

The material response changes according to the characteristics of the load. Indeed, by reducing the frequency of solicitation the polymer chains can reorganize themselves within a peculiar molecular motion characteristic by the time τ, comparable to the period T corresponding to the specified frequency, showing a typical rubbery behavior. If instead, the polymer chains do not have enough time to reorganize, when the stimulation's frequency is sufficiently high, it will reflect the glassy behavior which manifests physically as an increase in modulus as shown in Fig. 2.

The temperature assumes a crucial role in molecular deformation as well, affecting, according to the theory of free volume, the inter-molecular distance. Specifically, when the temperature increases, this distance increases as well, facilitating the movement of the polymeric chains and therefore reducing the storage modulus at a fixed frequency. Hence, from a macroscopic point of view, the temperature variation affects the material properties by determining a shift of its master curve which can be re-conducted to the frequency change based on the time-temperature superposition principle [42]. The value of the shift factor is determined according to specific laws, among which the most diffused, especially for polymer applications, is the Williams–Landel–Ferry one [43]. Due to the limitation of most commercial DMA equipment, the time-temperature superposition, above described, is usually used to describe the viscoelastic behavior at high or low frequencies, which is experimentally inaccessible. Using this principle, performing tests in a narrow range of frequencies and at different temperatures, it is pos-

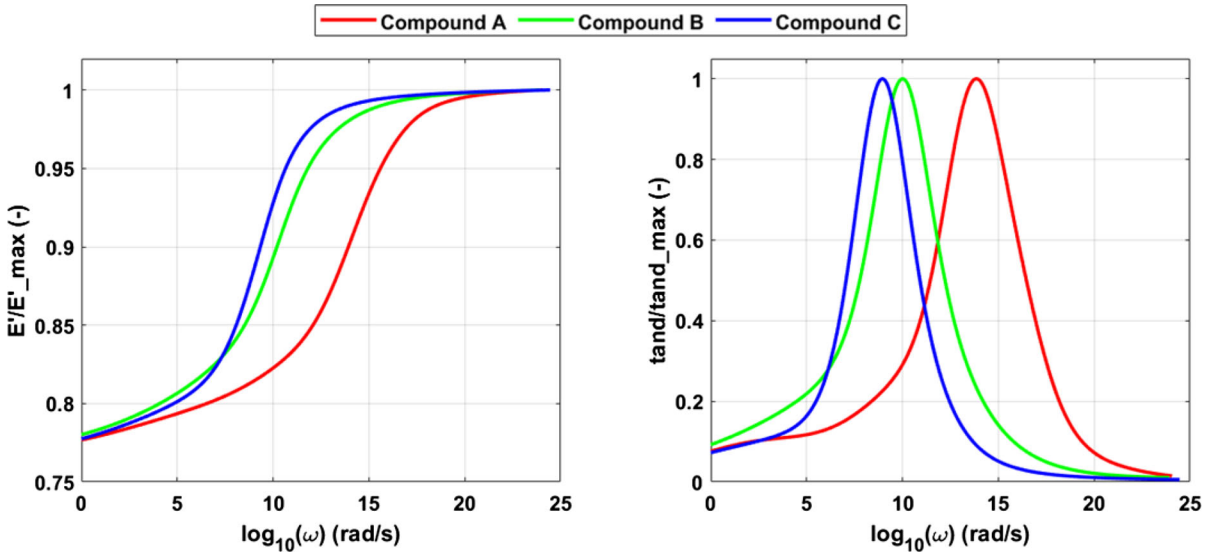

Fig. 2 Storage modulus (left) and loss factor (right) as a function of frequency for 3 different Compound A-B-C on a log-log scale, normalized with respect to the maximum value

sible, through an appropriate shift law, to reconstruct an entire master curve, which describes the behavior of the material on a large time-temperature scale.

2.2 Constitutive rheological elements

The correct modeling of the material viscoelastic properties is a key element in achieving reliable results from analytical models or finite-element-based analyses when designing with these types of materials. Several mathematical models can be found in the literature to help understand and describe material viscoelastic behavior [18], but it is important to emphasize that simple models like Maxwell (series of spring and dashpot) or Kelvin Voigt (parallel to spring and dashpot), fail to represent the complex non-linear response of viscoelastic materials in a large range of frequency. To improve these models and take into account the multiple characteristic times that these types of materials have, the generalized linear viscoelastic models are commonly used. These models consist of a connection of several Maxwell elements in parallel (Generalized Maxwell Model (GMW)) or several Kelvin–Voigt elements in series (Generalized Kelvin–Voigt Model (GKW)) and are able to overcome the limitations of simple viscoelastic models, allowing the reproduction of realistic trend of the material properties, with constant modulus at low and high frequencies, growing in the middle, and a phase which is nil at low and high frequencies and non-zero in the middle. However, these models are based on a large set of differential equations which increases considerably the computational load [44].

To reduce the number of parameters, an additional fundamental mechanical element, commonly known as spring-pot (Fig. 3), is introduced replacing the derivative's integer order with a fractional one within the dashpot's constitutive equation, which is described in Eq. (3):

$$\sigma(t) = C_\alpha \frac{d^\alpha \varepsilon(t)}{dt^\alpha} \tag{3}$$

where C_α represents the spring-pot coefficient and α is the properly identified fractional coefficient. This new element provides a novel and more realistic approach to the study of dissipating phenomena inside the solid material, helping to improve the performance of the GMW and resulting in a new robust formulation known as the Generalized Fractional Maxwell Model (GFMW). From a mathematical point of view, a generic constitutive equation for viscoelastic materials, based on fractional derivative orders, is reported in Eq. (4) [38]:

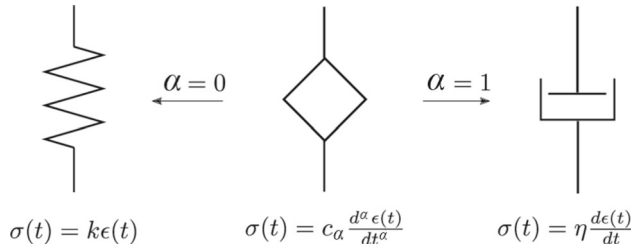

Fig. 3 Representation of rheological elements and their constitutive equations

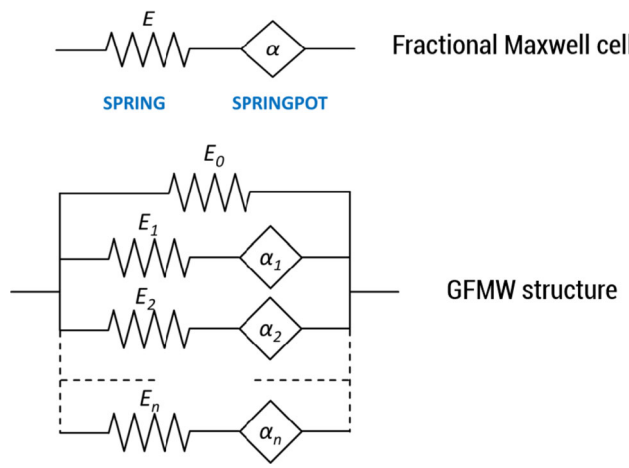

Fig. 4 Representation of the single fractional Maxwell cell and of the generalized fractional Maxwell model structure

$$\sum_{n=0}^{N} a_n \frac{d^{\alpha_n}\sigma(t)}{dt^{\alpha_n}} = \sum_{m=0}^{M} b_m \frac{d^{\beta_m}\epsilon(t)}{dt^{\beta_m}} \tag{4}$$

where α_n and β_m are the fractional derivative orders included within the range [0, 1]. In this study, dealing only with viscoelastic solids, it will be considered the Maxwell formulation with $N = M$ and $b_0 = 0$, with an isolated spring in parallel to the Maxwell cells to display also reversible creep [37]. Turning to the frequency domain by applying the Fourier transform and assuming that $a = b$, Eq. (4) gives the following expression for the complex moduli:

$$E^*_{i\omega} = K_0 + \sum_{i=1}^{N} \frac{K_i C_i (j\omega)^{\alpha_i}}{K_i + (j\omega)^{\alpha_i} C_i} \tag{5}$$

where ω is the frequency, which is strictly positive for the phenomenon under consideration, and the parameters K_i and C_i represent the spring stiffness and the spring-pot coefficients for each i-th element, respectively, as represented in Fig. 4.

2.3 Pole-zero transformation technique

The widely used GFMW has demonstrated great ability in predicting the viscoelastic behavior of materials. However, the employment of the GFMW approach in its classical form (Eq. 5), or its equivalent form in the frequency domain (Eq. 6), poses further challenges within the identification process of the parameters K_i and C_i due to their high variability relative to each other. This issue, compounded by an upper-non-limited existence domain comprehending positive real numbers, results in a substantial additional computational cost within the identification process. Indeed, it is highly likely that an optimizer may converge to a local minimum dependent on initial conditions rather than a global solution, thereby limiting the applicability of the GFMW approach.

$$Z(\omega) = K_0 + \sum_{i=1}^{N} \frac{(j\omega)^{\alpha}_i K_i C_i}{(j\omega)^{\alpha}_i C_i} \tag{6}$$

To overcome the above issues, the pole-zero approach proposed by Renaud et al. in [37] results to be extremely advantageous. Indeed, the identification process can be constrained to guarantee a relatively low variabil-

ity between different poles' and zeros' frequencies, therefore facilitating the consequent optimization process. The numerical optimization is advantageously constrained imposing the alternation of poles p and zeros z (Eq. 7) according to the third property demonstrated by Bland [12] for linear dissipate systems:

$$z_1 < p_1 < \ldots < z_i < p_i < \ldots < z_N < p_N \tag{7}$$

Once obtained the poles' and zeros' frequencies, Maxwell's parameters are transformed employing the Eqs. 8 and 9:

$$K_i = K_0 \prod_{h=1}^{N} \left(\frac{\omega_{p,h}}{\omega_{z,h}} \right) \frac{\omega_{z,h} - \omega_{p,i}}{\omega_{p,h}(1 - \delta_{ih}) - \omega_{p,i}} \tag{8}$$

$$C_i = \frac{K_i}{\omega_{p,i}} \tag{9}$$

where the parameters K_i and C_i are uniquely described:

- K_0 is the stiffness of the isolated spring;
- K_i and C_i represent the stiffness and the spring-pot coefficients;
- $\omega_{p,i}$ and $\omega_{z,h}$ are the frequencies of poles p and zeros z, respectively;
- δ is the Kronecker delta, which is assumed null except when $i = h$ where $\delta = 1$ is imposed.

According to this formulation, Dion et al. in [45] and [46] manipulated the original form of the Generalized Maxwell model to obtain a new formulation in the poles-zero form, as shown in the Eq. (10):

$$Z(\omega) = K_0 \prod_{i=1}^{N} \frac{1 + (\frac{j\omega}{\omega_{z,i}})}{1 + (\frac{j\omega}{\omega_{p,i}})} \tag{10}$$

3 Material modeling approaches

3.1 GFMW model limitations and multi-objective optimization

In literature, different approaches are available to address multi-objective optimization, mainly employing a posterior method to generate the Pareto optimal solutions and to search for the most suitable trade-off solution [47,48]. The intrinsic conflict between error-defined cost towards the two completely diverse material properties (storage modulus and loss factor) becomes evident that finding an optimal solution is intricate, necessitating a compromise between the response towards two completely different physical quantities.

The well-known NSGA-II algorithm proposed by K.Deb et al. [49], rapidly becoming the most widely used technique, has been chosen for the optimization scope [50]. Employing a normalized value necessary for comparing different curves with varying magnitudes, the mean absolute percentage error (MAPE) offered the best-fitting results. MAPE definitions are reported in Eq. (11), where the MAPE errors consider the model predictions (indicated with a hat) and the experimental data in terms of storage modulus, E', and loss factor, $\tan\delta$.

$$\begin{aligned} \mathrm{MAPE}_{E'} &= \frac{1}{n} \sum_{i=1}^{n} \left| \frac{E'_i - \hat{E}'_i}{E'_i} \right| \times 100\% \\ \mathrm{MAPE}_{\tan(\delta)} &= \frac{1}{n} \sum_{i=1}^{n} \left| \frac{\tan(\delta)_i - \hat{\tan}(\delta)_i}{\tan(\delta)_i} \right| \times 100\% \end{aligned} \tag{11}$$

A result of a calibration performed employing the NSGA-II algorithm with the previously described GFMW model, widely employed in literature for the description of viscoelastic materials, is presented in Fig. 5. As it can be easily observed, the set of obtainable parameters (and therefore the resulting model's response) deeply depends on the definition of the error-cost function within the multi-objective routine.

As it appears evident in Fig. 5, the chosen material's model is capable of correctly predicting storage modulus and loss factor behavior separately. However, imposing that the two errors have to guarantee similar dimensions, the GFMW approach is currently unable to approximate storage modulus and loss factor trends simultaneously, showing larger deviations, especially around the glass transition of the storage module and the peak of the loss factor.

Another limitation is observed for the materials exhibiting a greater variability of storage modulus at lower frequencies, as in the case of the material's storage modulus represented in Fig. 1, where the already widely adopted model is not able to reproduce the experimental trend.

In response to these challenges, a novel approach to the study of the general Maxwell model will be intro-

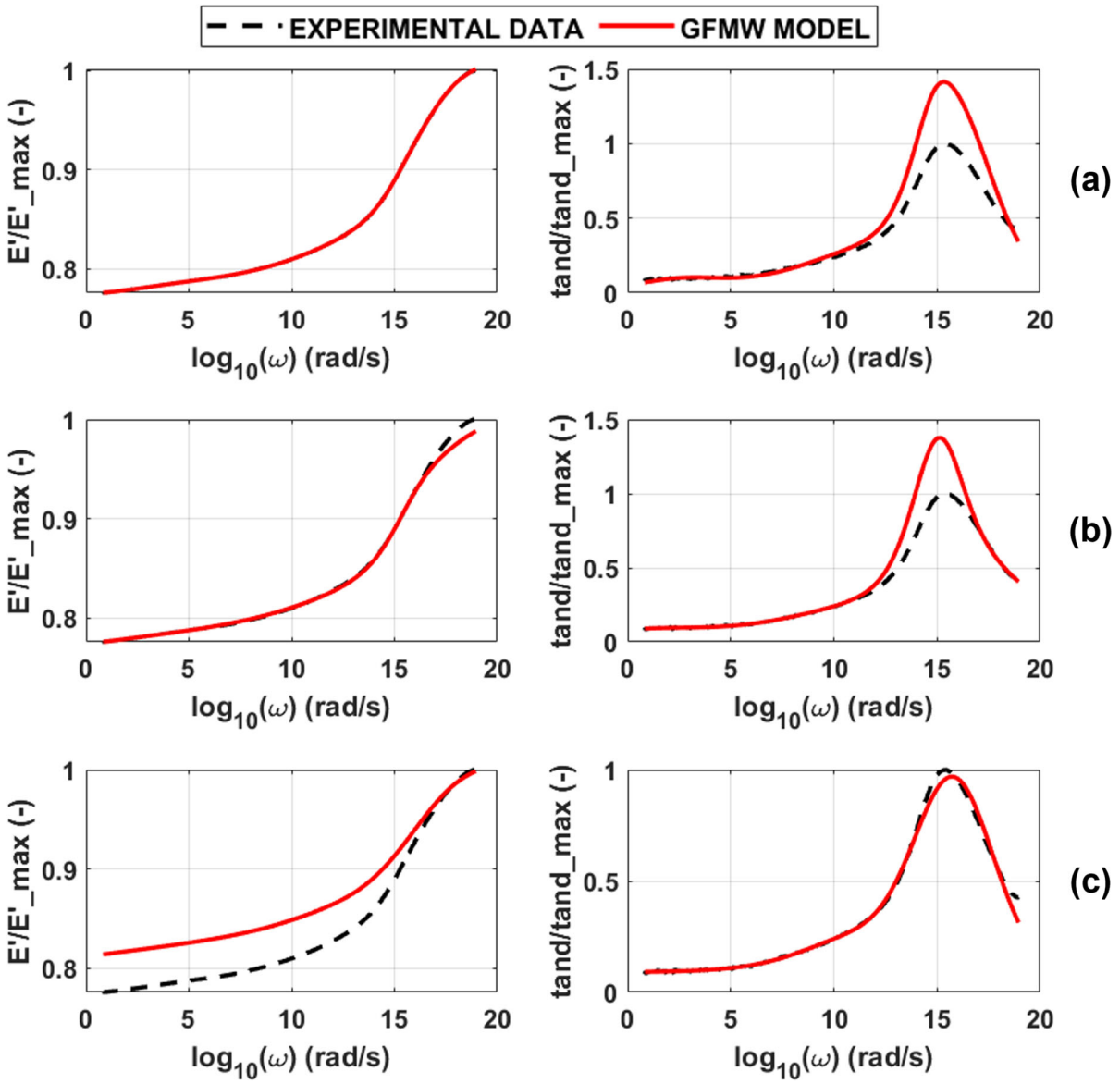

Fig. 5 Model response towards storage modulus (left) and loss modulus (right) for a generic tire polymer. Error function definitions: **a** major weight for E', **b** same weights for E' and $\tan\delta$, and **c** major weight for $\tan\delta$

duced in the next section. This approach extended the GFMW by adopting a nonlinear approach allowing to increase the model's flexibility and an improved accuracy towards addressing the limitations encountered with the GFMW model.

3.2 Nonlinear Maxwell model

In real materials, the transition phase between rubbery and viscoelastic behavior appears often less clear than the one represented in Fig. 6, with one or more slope

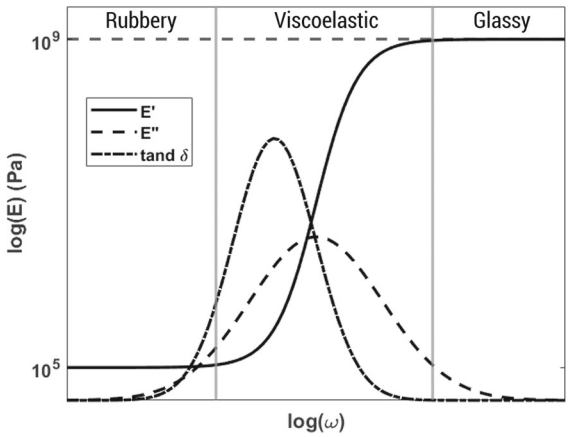

Fig. 6 Ideal trend of complex moduli G_1, G_2 and loss factor $\tan\delta$

variations related to the complex internal dissipative phenomena in the material. Viscoelastic materials, as above described, are strongly influenced by their chemical composition. The intermolecular forces, the length of the polymer chains, the curing, and the crystalline degrees are all factors that interact with each other, generating an overall material response depending on the speed at which the stress is applied.

In general, it can be observed that, while the loss factor keeps its bell shape, for the storage modulus the sigmoidal trend is altered by rapid changes in slope as the frequency increases; i.e, in the example reported in Fig. 1 it is evident that for frequencies of the order of 10^6, there is an inflection point, where some movements, previously possible with a relatively slow application of stress, are now blocked, generating an increase in terms of the storage modulus slope. In particular, this phenomenon can be understood by observing its temperature dependence. The compounds, a mixture of polymers, oil, resin, and additives, exhibit varying properties at different temperatures due to the distinct impacts of each component. Typically, it is observed that until a specific characteristic temperature is reached, the rheological behavior of the compound correlates with that of the polymers, which are the principal components. At higher temperatures, the resin begins to exert a greater influence as certain chemical balances change, resulting in increased freedom of movement of the polymer chains and a more pronounced reduction in the storage modulus [51]. Since this variability is strongly influenced by the chemical characteristics, which may also vary depending on the technological treatment undergone, it is difficult to approximate using a linear formulation.

Hence there is the need to take into account a nonlinear approach, already proposed by Jrad et al. [41], who first considered a non-linear spring element, with variable stiffness as a function of the stress amplitude, in parallel with Maxwell's elements to approximate the experimental trend of acquired dynamic characteristics. The approach presented in this work aims to increase flexibility in following slope variations; for this reason, non-linearity is initially introduced in the isolated spring K_0, which has greater influence precisely at low frequencies, by introducing the dependence on omega by means of a function $K(\omega)$. This will increase the flexibility of the model in the approximation of the storage modulus by being able to predict the slope variations associated with complex chemical structures. To justify the proposed formulation, a mathematical validation of pole and zero expression with this new nonlinear element must be specifically addressed. In this section, it will be demonstrated the validity of the equation in the case of two elements of Maxwell in parallel with an isolated nonlinear spring, as it will show that the result may be easily extended to n elements.

By considering the Eq. (10) with $n = 2$, it is possible to obtain:

$$Z(\omega) = K_0(\omega)\left(\frac{1+(\frac{j\omega}{\omega_{z,1}})}{1+(\frac{j\omega}{\omega_{p,1}})}\right)\left(\frac{1+(\frac{j\omega}{\omega_{z,2}})}{1+(\frac{j\omega}{\omega_{p,2}})}\right) \tag{12}$$

$$Z(\omega) = K_0(\omega) * (j\omega) * \frac{\omega_{p,1}}{\omega_{z,1}} * \frac{\omega_{z,1}+j\omega}{\omega_{p,1}+j\omega} * \frac{\omega_{p,2}}{\omega_{t,2}} * \frac{\omega_{z,2}+j\omega}{\omega_{p,2}+j\omega} * \frac{1}{j\omega} \tag{13}$$

and taking into account:

$$\begin{aligned} A_0 &= \frac{\omega_{z,1}}{\omega_{p,1}}\frac{\omega_{z,2}}{\omega_{p,2}} \\ A_1 &= \frac{\omega_{z,1}-\omega_{p,1}}{-\omega_{p,1}}\frac{\omega_{z,2}-\omega_{p,1}}{\omega_{p,2}-\omega_{p,1}} \\ A_2 &= \frac{\omega_{z,2}-\omega_{p,2}}{-\omega_{p,2}}\frac{\omega_{z,2}-\omega_{p,1}}{\omega_{p,1}-\omega_{p,2}} \end{aligned} \tag{14}$$

the Eq. (13) can be rewritten in a different form as follows:

$$
\begin{aligned}
Z(\omega) =& K_0(\omega) * (j\omega) * \frac{\omega_{p,1}}{\omega_{z,1}} * \frac{\omega_{p,2}}{\omega_{z,2}} * \\
& \left[\frac{A_0}{j\omega} + \frac{A_1}{j\omega + \omega_{p,1}} + \frac{A_2}{j\omega + \omega_{p,2}}\right] \\
=& K_0(\omega) * \left[1 + \frac{A_1 A_0^{-1} j\omega}{j\omega + \omega_{p,1}} + \frac{A_2 A_0^{-1} j\omega}{j\omega + \omega_{p,2}}\right]
\end{aligned} \tag{15}
$$

Considering the relationship between pole and zero formulation and spring K_i and dashpot C_i elements:

$$
K_i(\omega) = K_0(\omega) \prod_{h=1}^{N} \left(\frac{\omega_{p,h}}{\omega_{z,h}}\right) \frac{\omega_{z,h} - \omega_{p,i}}{\omega_{p,h}(1 - \delta_{ih}) - \omega_{p,i}} \tag{16}
$$

$$
C_i(\omega) = \frac{K_i(\omega)}{\omega_{p,i}} \tag{17}
$$

with $i = [1, 2]$, it is possible to obtain the original form of the generalized Maxwell model reported in Eq. (6) with $n = 2$:

$$
Z(\omega) = K_0(\omega) + \frac{j\omega K_1 C_1}{K_1 + j\omega C_1} + \frac{j\omega K_2 C_2}{K_2 + j\omega C_2} \tag{18}
$$

The non-linear spring proposed has a different response depending on the frequency, but the response remains simultaneous with the solicitation. From a mathematical point of view, the associated impedance of this element remains a pure real element if the following condition is respected:

$$
K_0(\omega) : \omega \in \mathbb{R}^+ \rightarrow K_0(\omega) \in \mathbb{R}^+ \tag{19}
$$

Therefore, it is possible to assert that the variability of the stiffness K_0 amplifies both the real and imaginary parts of the equivalent impedance, generating a change in the modulus of the latter without changing its phase. In other words, the non-linear equation introduced into the K_0 modifies the trend of the storage modulus without changing the loss factor's prediction, in line with [37].

To this end, it is necessary to ensure that the previous Eqs. (8 and 9) are satisfied, which is achievable by assuming that the nonlinearity expands beyond the solitary spring in parallel. This means that it is reasonable to consider all elements of the system became nonlinear elements, in particular, nonlinear springs or nonlinear fractional springpots whose constants can be described respectively by the Eqs. (16 and 17). Based on this consideration, the performance of the model can be improved by continuing to use the pole and zero formulation. These changes, as will be shown, will have a significant impact on the adaptability of this model for materials of a different nature.

3.3 Nonlinear generalized fractional Maxwell model (NLGFMW)

It is worth noticing that pole and zero formulation can be generalized to fractional calculus as done by Renault et al. [37] as follows:

$$
Z(\omega) = K_0 \prod_{i=1}^{N} \frac{1 + (\frac{j\omega}{\omega_{z,i}})^{\alpha_i}}{1 + (\frac{j\omega}{\omega_{p,i}})^{\alpha_i}} \tag{20}
$$

where α_i is the derivative fractional index of the springpot into the Maxwell element i-th and it is a real number between 0 and 1. According to this formulation, the modulus and the phases of this fractional calculus pole-zero formulation are given by the equations:

$$
|Z(\omega)| = K_0 \prod_{i=1}^{N} \frac{\sqrt{1 + 2\left(\frac{\omega}{\omega_{z,i}}\right)^{\alpha_i} cos\left(\frac{\gamma\pi}{2}\right) + \left(\frac{\omega}{\omega_{z,i}}\right)^{2\alpha_i}}}{\sqrt{1 + 2\left(\frac{\omega}{\omega_{p,i}}\right)^{\alpha_i} cos\left(\frac{\gamma\pi}{2}\right) + \left(\frac{\omega}{\omega_{p,i}}\right)^{2\alpha_i}}} \tag{21}
$$

$$
\begin{aligned}
\delta = & \sum_{i=1}^{N} tan^{-1}\left(\frac{\left(\frac{\omega}{\omega_{z,i}}\right)^{\alpha_i} sin\left(\frac{\gamma\pi}{2}\right)}{1 + \left(\frac{\omega}{\omega_{z,i}}\right)^{\alpha_i} sin\left(\frac{\gamma\pi}{2}\right)}\right) \\
& - tan^{-1}\left(\frac{\left(\frac{\omega}{\omega_{z,i}}\right)^{\alpha_i} sin\left(\frac{\gamma\pi}{2}\right)}{1 + \left(\frac{\omega}{\omega_{p,i}}\right)^{\alpha_i} sin\left(\frac{\gamma\pi}{2}\right)}\right)
\end{aligned} \tag{22}
$$

In summary, the previously proposed solutions can be updated to take into account the mentioned nonlinear components using the mathematical steps described above the Eq. (22) continues to be valid for the calculus of the phase, the following equation will be valid for the modulus:

$$
|Z(\omega)| = K_0(\omega) \prod_{i=1}^{N} \frac{\sqrt{1 + 2(\frac{\omega}{\omega_{z,i}})^{\alpha_i} cos(\frac{\gamma\pi}{2}) + (\frac{\omega}{\omega_{z,i}})^{2\alpha_i}}}{\sqrt{1 + 2(\frac{\omega}{\omega_{p,i}})^{\alpha_i} cos(\frac{\gamma\pi}{2}) + (\frac{\omega}{\omega_{p,i}})^{2\alpha_i}}} \tag{23}
$$

It should be noted that being the non-linearity based on the same stiffness equation $K_0(\omega)$, the number of parameters to be considered is limited. In other words, in addition to the usual $3n+1$ parameters in the GFMW, only the parameters of the single nonlinear equation need to be added.

In detail, since the additional stiffness K_0 influences the storage modulus, from a physical point of view it is reasonable to think that it has a trend resulting from

the variation in stiffness of the viscoelastic materials as the frequency varies. Namely, as previously explained, there are two characteristic slope variations in the storage modulus, more or less marked, which reflect the evolution of the behavior of these materials as the frequency increases, linked to phenomena intrinsic to the material itself. In this context, the glass transition temperature T_g assumes particular importance as it marks the transition from a rubbery to a glassy behavior with a stabilization of the stiffness at a very high value. Therefore, in this study, a bell-shape trend for the $K_0(\omega)$ has been assumed, with the pick corresponding to the T_g value, and shape factors adjusted based on experimental data.

The function $K_0(\omega)$ is composed of the sum of two Gaussian functions that ensure the bell-shaped form, both centered on a reference value of frequency ω^* chosen, as stated above, as the glass transition frequency (see Eqs. 24 and 25). This step allowed to reduce the parameters of each Gaussian from 3 to 2, making the identification faster and more robust. The parameters to embed with classical GFMW and governing the function $K_0(\omega)$ became 5 with the addition of the asymmetry parameter t (Eq. 24), which handles the different behavior required of the spring at low and high frequencies, as illustrated in Fig. 8. So, the final form of the K_0 is of the following type:

$$\begin{cases} K_0(\omega) = f_1(a,b) + f_2(c,d) & \text{if } \omega < \omega^* \\ K_0(\omega) = t \cdot (f_1(a,b) + f_2(c,d)) + shift & \text{if } \omega > \omega^* \end{cases} \tag{24}$$

with:

$$\begin{cases} f_1(a,b) = a \cdot e^{(\frac{\omega-\omega^*}{b})^2} \\ f_2(a,b) = c \cdot e^{(\frac{\omega-\omega^*}{d})^2} \end{cases} \tag{25}$$

This structure provides a well-defined meaning to the functions f_1 and f_2; in fact by constraining b>>d and a<c, as imposed into the algorithm, f_1 governs the functions far from the glass transition frequencies, while f_2 characterizes the non-linear spring behavior near these frequencies, an example is shown in the graph in Fig. 7. So, the global role of each parameter, also shown in the sensitivity analysis in Fig. 8, is reported below:

- a is the dimension factor which, in conjunction with parameter c, handles the orders of magnitude of the curve

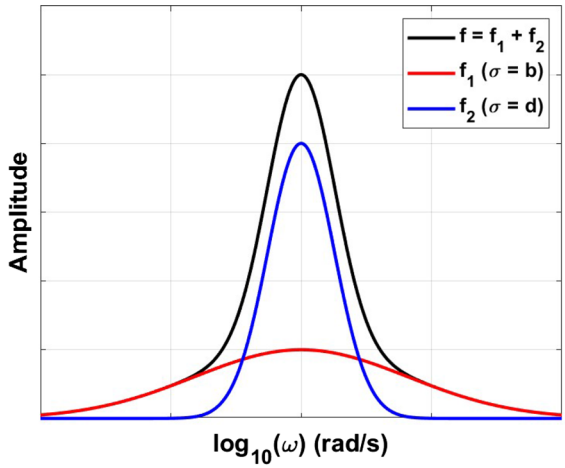

Fig. 7 Example of the sum of the functions f_1 and f_2

- b is the shape parameter at external frequencies which affects the two asymptotes at low and high frequencies
- c is the growth factor which affects the ordinate of the peak
- d is the shape factor at intermediate frequencies which governs the extension of the peak and the position of the inflection points on the x-axis of the bell shape

Finally, the shift is automatically determined by the software to ensure the class C^2 continuity of the function.

4 Results

The proposed NLGFMW model has been employed to reproduce the dynamics moduli of 10 different viscoelastic materials for tire applications, covering a wide range of different behaviors, to discover the minimum number of elements to employ in the domain of interest, and therefore the number of parameters sufficient to correctly reproduce the desired characteristics. In the following paragraphs, a detailed description of the materials analyzed is provided. Subsequently, a comparative evaluation of novel versus traditional model performance is undertaken, including a thorough analysis of the total number of parameters needed and considerations about the processing run-time. These aspects were instrumental in developing a logical operational diagram for the NLGFMW calibration algorithm. Finally, the potential of this model is discussed,

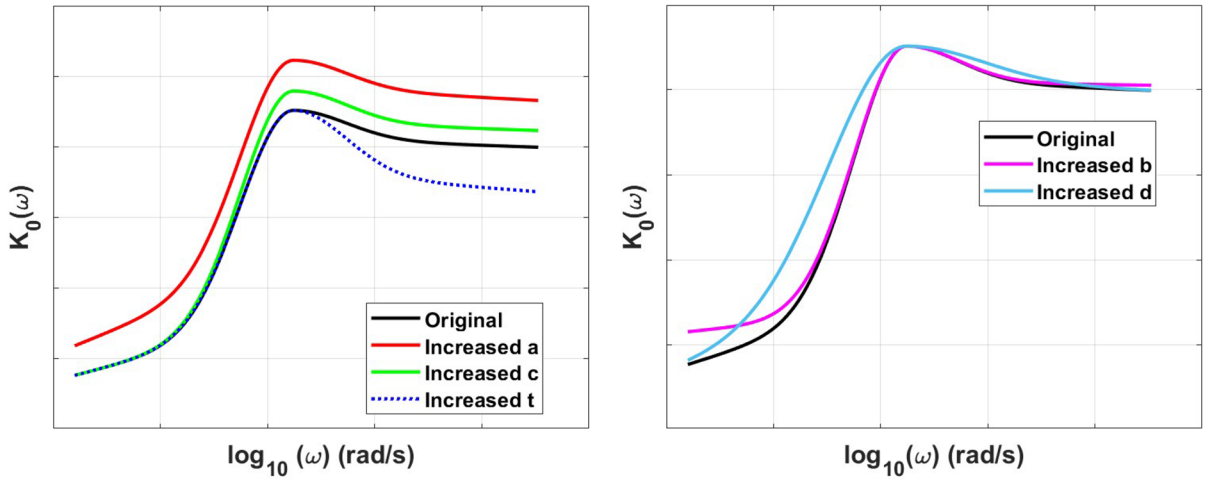

Fig. 8 Change of K_0 of tipical trend as a consequence of the increase of each five parameters

demonstrating its efficacy even with limited experimental data.

4.1 Materials

The 10 materials selected were chosen to ensure sufficiently differentiated mechanical properties to cover a wide range of viscoelastic responses without going into the details of the chemical nature, which was irrelevant to the study. The storage modulus and the loss tangent were evaluated for each of these compounds through DMA testing performed with a tensile geometry and horizontal orientation, at a reference frequency of 1Hz [13,52,53]. The chosen test mode was the temperature sweep, in a range between -50°C and 120°C (with air cooler), with a temperature ramp of 1°C/min and a % strain of 0.1. Each material was tested under the same conditions, in oscillator strain control mode with an amplitude of 0.05%, and applying a static force of 2N with a force resolution of $10^{-6}N$, a tanδ resolution of 10^{-6} and a modulus resolution of $10^{-5}Pa$. The data delivered by the DMA provider also included the frequency data obtained with an appropriate shift law based on the Time-Temperature Superposition Principle.

In detail, the viscoelastic materials present different glass transition frequencies and viscoelastic proprieties, summarized in Table 1. The table reports the value of frequency in which the peak of loss factor is obtained, along with the corresponding value, dimensionless respect to the minimum of this group, and the stabilized value of the storage modulus in the glass zone (E'_∞), also dimensionless respect to the minimum value (the presence of the normalized value is necessary for confidentiality reasons). These compounds show, in general, dynamic module plateaus at low and high frequencies with different slopes, based on their diversified microscopic composition. In the following, these elements will be indicated as Compounds A, B, and C, with particularly marked transition zones and high value of glass region plateau with E'_∞ 4 order of magnitude greater respect the lowest; Compounds D, E and F show a not very pronounced first transition at low frequencies and relatively low glass transition frequencies, similar to each other but with different value of loss factor and storage modulus reached. Finally, Slabs A, B, C, and D are characterized by a higher frequency of glass transition and low values of both the loss factor and storage modulus.

4.2 NLGFMW application with DMA test

The identification procedure, needed to find the optimal set of parameters, including poles, zeros, and the K_0 parameters, was performed with different numbers of fractional elements and the results were compared both qualitatively with graphs and quantitatively with the MAPE metrics, both for the storage modulus and the loss factor, employing the metrics defined in Eq. (11).

Table 1 Characteristics of materials under investigation

Material	tan(δ) Peak frequency (Hz)	Relative max(tan(δ))	Relative E'_∞
Compound A	13.9	1.17	4.23
Compound B	9.9	1.31	4.36
Compound C	8.9	1.64	4.32
Compound D	7.7	1.88	1,59
Compound E	8.1	1.48	1,55
Compound F	8.2	1.50	1
Slab A	15.4	1	1.50
Slab B	13.8	1.12	1.14
Slab C	13.7	1.12	1.45
Slab D	12.1	1.26	1.45

frequency is in log_{10} scale; data in columns 3 and 4 are normalized against the minimum value in the column

It is worth specifying that, in the NLGFMW model, the total number of parameters is determined by the number of fractional elements introduced and the function $K_0(\omega)$. In total, there are 3 parameters for each element and 5 parameters of the $K_0(\omega)$.

Figure 9 shows the results of the model implementation with 3, 4, and 5 elements, and, respectively, with 14, 17, and 20 parameters, for four different materials, while in Table 2, the MAPE errors, evaluated for all the samples available, are reported. Note that in all figures the properties will be dimensionless to the maximum value to maintain the confidentiality of the data used.

Analyzing the results, shown in Table 2, it is evident that all three NLGFMW models exhibit satisfactory performance across all ten materials considered, with a maximum error of approximately 7% observed for both the storage modulus E' and the loss factor tan δ. Generally, increasing the number of elements leads to lower error rates and thus to a better representation of real data, but also to a higher computational cost and number of parameters to identify. Nevertheless, it is noteworthy that in certain instances, as for the compound F, the 5-elements NLGFMW model demonstrates inferior performance compared to its 4-elements counterpart, probably because the number of parameters is too high compared to the amount of data available, leading to less efficient identification of poles and zeros. Considering a trade-off between the goodness of the model and the computational load of the calibration procedure, the 4-elements NLGFMW model is revealed to be the optimal choice.

It is interesting to compare the results of the newly-developed nonlinear fractional model with the already widely adopted fractional model, which proved to give similar results to the generalized Maxwell model, but with a limited number of parameters, thus reducing the computational load that affects efficiency and effectiveness [38]. For the comparison, to guarantee a comparable number of parameters, 3-elements were adopted for the nonlinear NLGFMW model (14 parameters to identify), while 4-elements were used for the linear GFMW model (thus 13 parameters to identify).

The outcomes are reported graphically for four materials in Fig. 10, together with the corresponding MAPE metrics reported in Table 3, chosen as the goodness criteria since it proved to be the most robust methodology as the number of elements changes.

The compounds A, B, and C show excellent results already with the previous GFMW model, as reported in the previous study since these materials exhibit a very regular trend for the viscoelastic properties, with marked transition zones. However, the classical fractional generalized Maxwell model does not work optimally with the other materials which show a less predictable trend of the viscoelastic moduli. In particular, the model can return a good fitting only of one of the properties, while the other one is not acceptable. Also changing the weight on the errors, the result is to improve the property not well fitted and worsen the other. This is the reason that forced the authors to the introduction of a nonlinear spring, as explained before, which permits the achievement of excellent results both on the storage modulus and the loss factor.

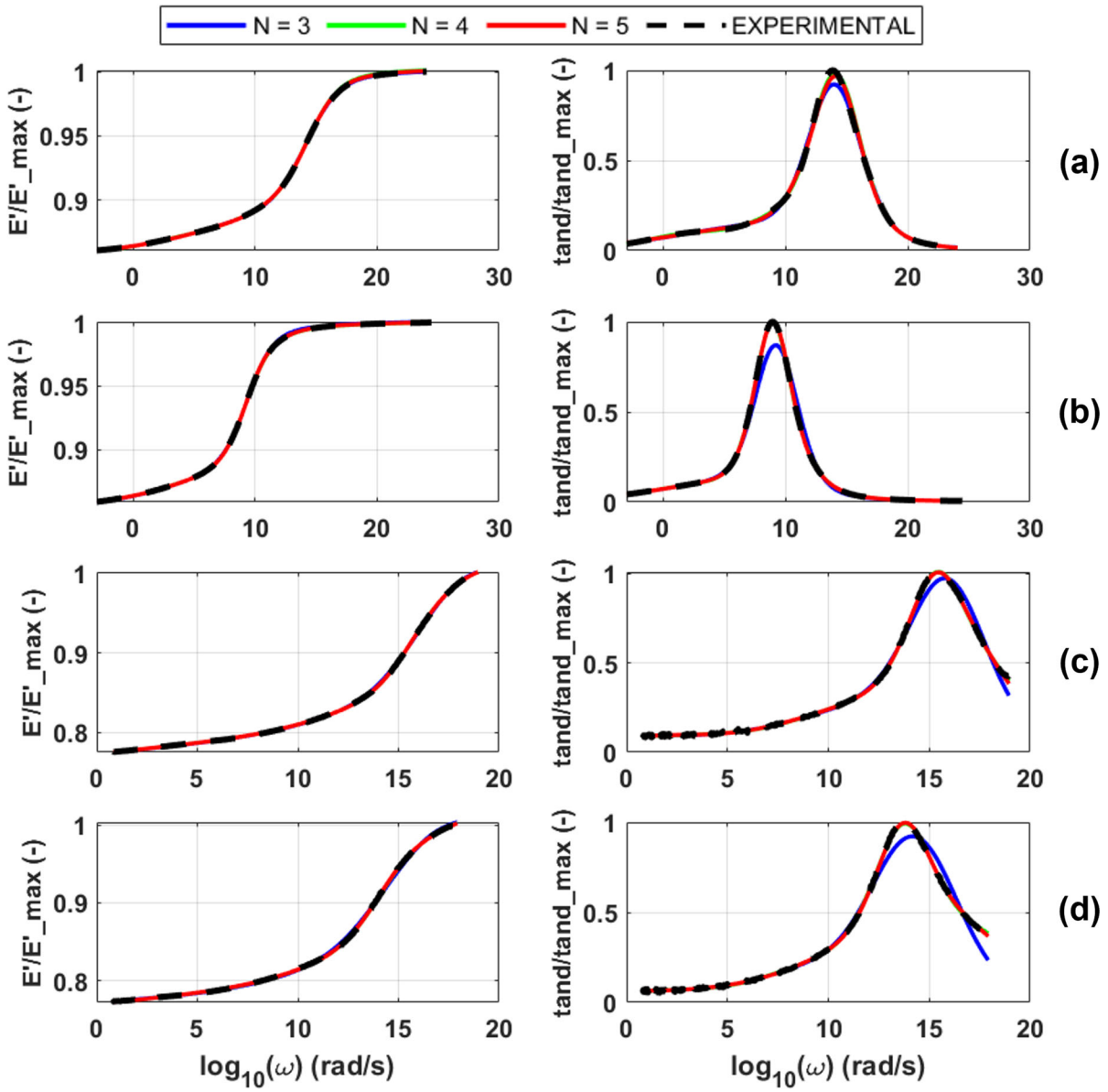

Fig. 9 E' and $\tan\delta$ curves reproduced with NLGFMW models composed of 3, 4, and 5 elements, for Compound A (**a**), Compound C (**b**), Slab A (**c**) and Slab C (**d**)

From the previous analysis, it appears evident that the nonlinear NLGFMW model proposed with 4 fractional Maxwell cells can reproduce efficiently all the materials' viscoelastic properties under investigation. However, on some occasions, the non-linearity K_0 is not strictly essential, since the classical fractional GFMW model is able to achieve satisfactory results. For this reason, the algorithm methodology described in Fig. 11 is designed as the general approach to model the frequency-temperature dependent behavior of viscoelastic materials for tire applications, where the nonlinear $K_0(\omega)$ initially considers its constant term and the other 3 parameters are identified only if specific criteria are met.

As concerns the running time these are calculated with the following PC'setup: processor Intel I-7 13th gen with cores speed (6P+8E) around 4GHz, 32 Gb DDR5 ram and the Matlab 2023b software with *fmin-*

Table 2 MAPE benchmark for NLGFMW models composed of 3, 4 and 5 elements

	3-elements NLGFMW		4-elements NLGFMW		5-elements NLGFMW	
Material	MAPE E' (%)	MAPE tan δ (%)	MAPE E' (%)	MAPE tan δ (%)	MAPE E' (%)	MAPE tan δ (%)
Compound A	0.526	4.023	1.363	1.532	0.986	3.421
Compound B	0.775	5.381	0.971	4.808	0.207	0.650
Compound C	1.541	5.173	0.096	0.509	0.188	0.814
Compound D	6.379	4.087	3.933	3.839	4.293	4.050
Compound E	5.204	3.882	4.470	3.617	3.961	2.929
Compound F	1.907	3.780	1.930	3.904	1.962	4.040
Slab A	1.006	3.213	0.820	2.154	0.803	2.175
Slab B	1.885	3.074	1.860	3.006	1.864	3.048
Slab C	1.822	4.703	1.104	2.937	1.147	2.891
Slab D	3.118	6.788	3.136	6.818	3.886	5.594

Table 3 MAPE benchmark for NLGFMW model composed of 3 elements (14 parameters) and GFMW model composed of 4 elements (13 parameters)

	3-elements NLGFMW		4-elements GFMW	
Material	MAPE E' (%)	MAPE tan δ (%)	MAPE E' (%)	MAPE tan δ (%)
Compound A	0.526	4.023	0.359	1.035
Compound B	0.775	5.381	0.238	1.529
Compound C	1.541	5.173	0.009	0.079
Compound D	6.379	4.087	16.853	16.318
Compound E	5.204	3.882	31.491	3.662
Compound F	1.907	3.780	24.652	3.737
Slab A	1.006	3.213	6.932	4.109
Slab B	1.885	3.074	10.280	3.233
Slab C	1.822	4.703	2.402	8.246
Slab D	3.118	6.788	19.322	5.735

con [54] as optimizer solving non-linear constrained optimization problems. The running times are reported in Table 4, and show how the 3-element model has a significant improvement over the 5-element, with times reduced by up to 48% in the case of the compound D. In general, the average processing time of the algorithm for the 3-elements model in this experimental campaign is 48% faster then 5-elements with a maximum under 3 s. These results increase the potentiality of this approach, making the model also suitable for real-time evaluations or implementations in material structure monitoring devices.

In detail, the general NLGFMW model is composed of 4 fractional Maxwell cells plus the $K_0(\omega)$ function, for a total of 17 parameters. The first identification is performed by activating just 1 parameter for the spring, which means a constant stiffness value and a total of 13 parameters. If the MAPE metrics both for E' and tan δ are less than a threshold (fixed at 10%), the model is already considered acceptable; otherwise, the other 3 $K_0(\omega)$ parameters are activated, with the stiffness varying with ω, so to calibrate the entire set of 17 parameters. Following this phase, a model reduction to 3 cells is attempted, to evaluate whether, with an even smaller number of parameters, the results are still valid. Also in this case, the acceptance or otherwise of the NLGFMW model is established based on the MAPE error threshold, which is set at 10% for both dynamic modules.

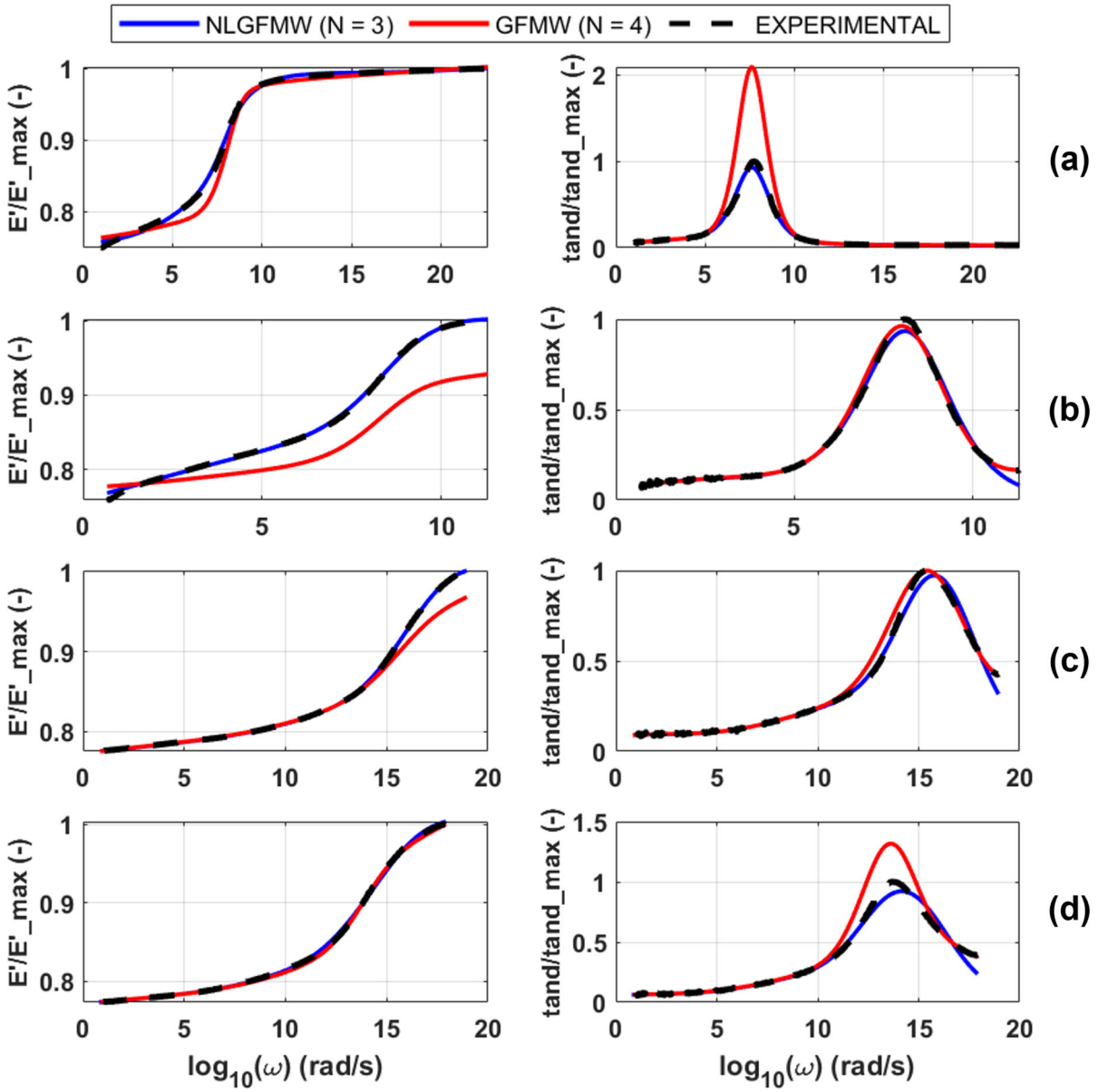

Fig. 10 Comparison in terms of E' and $\tan\delta$ fitting with a 3-elements NLGFMW model and a 4-elements GFMW model, for the following materials: Compound D (**a**), Compound E (**b**), Slab A (**c**), and Slab C (**d**)

In summary, therefore, the proposed NLGFMW model differs from those commonly employed in the literature due to the addition of the frequency dependence of the stiffness of the single spring of the Maxwell fractional model, which makes the model more versatile and able to reproduce the behavior of a wider range of viscoelastic materials.

4.3 Results addendum: NLGFMW application with limited experimental data

The results exposed so far have demonstrated that the non-linear fractional Maxwell model, expressed in the pole-zero domain, enables an excellent reproduction of the viscoelastic moduli in the frequency domain, validated for very different materials.

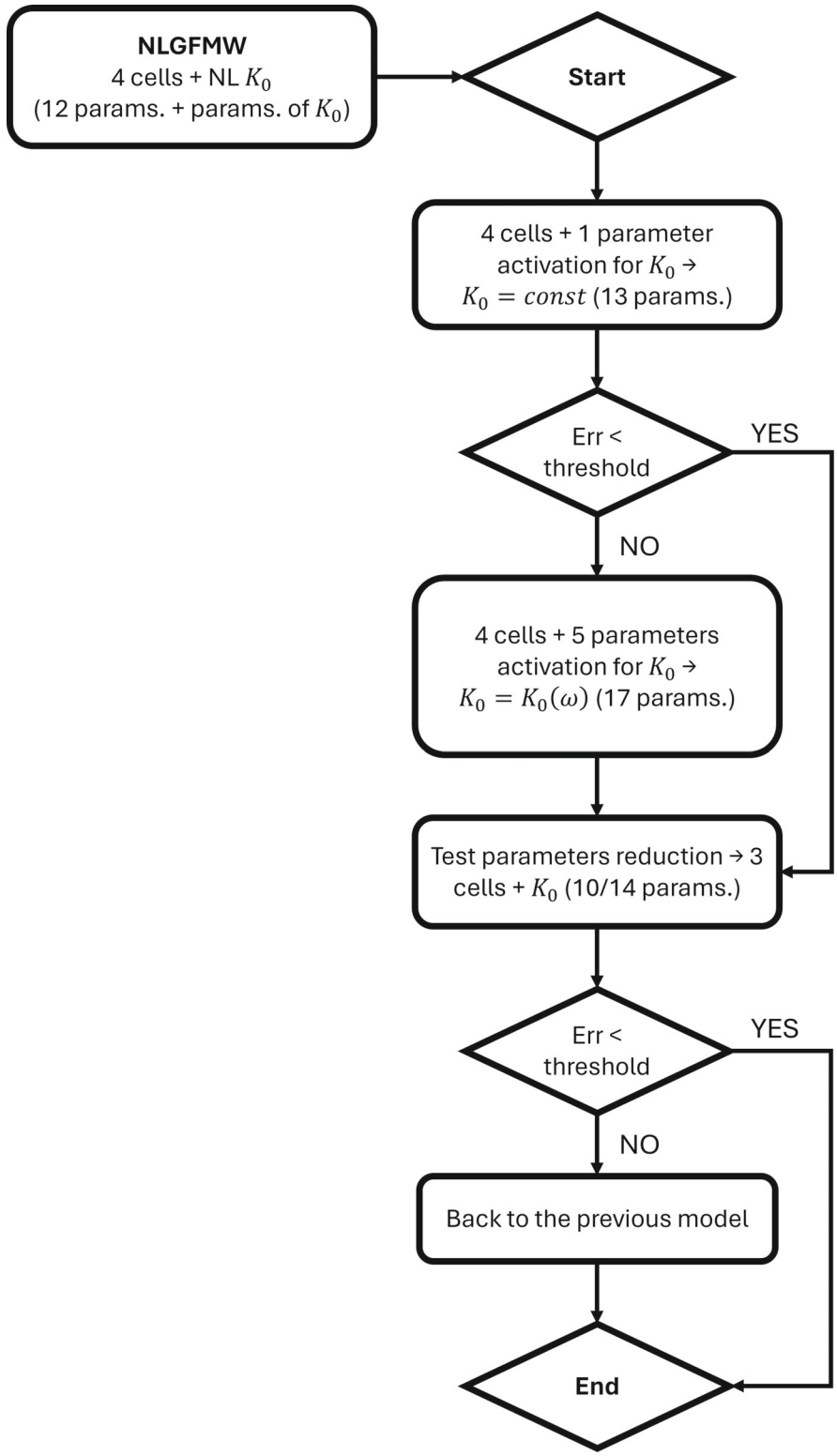

Fig. 11 Logical operaring diagram of NLGFMW calibration algorithm

Table 4 Running time for NLGFMW models composed of 3, 4, and 5 elements

	RUNNING TIME (s)		
Material	3-elements NLGFMW	4-elements NLGFMW	5-elements NLGFMW
Compound A	2.7	3.4	4.4
Compound B	2.5	3.5	4.4
Compound C	2.7	3.4	4.3
Compound D	2.3	3.2	4.4
Compound E	1.7	2.4	2.8
Compound F	1.6	2.2	2.8
Slab A	1.6	2	2.6
Slab B	1.3	1.9	2.5
Slab C	1.6	2.2	2.6
Slab D	1.3	2	2.5
Average	1.9	2.6	3.3
MIN | Relative MIN (%)	1.3 | 68%	2 | 76%	2.5 | 75%
MAX | Relative MAX (%)	2.7 | 142%	3.4 | 130%	4.4 | 133%

Taking into account that the amount of necessary resources, both in terms of money and time, increases as the range of frequencies to be tested experimentally expands, another interesting analysis conducted by the authors regards the possibility of calibrating the NLGFMW model employing a minimum number of experimental data. Similarly to the previous study of Genovese et al. [38], the best combination to correctly identify the viscoelastic master curves is composed of 5 zones: data corresponding to the lower and upper frequencies plateau of the storage modulus, the peak of the loss tangent curve, and the data from the curvature change of both curves. Genovese et al. also demonstrated that it is possible to obtain valuable results in reproducing the entire behavior of the material with just 3 zones: data corresponding to the lower and upper frequencies plateau of the storage modulus, and the peak of the loss tangent curve. The latter is the approach followed in this study, choosing experimental data that represent the low and upper-frequency plateaus, plus a zone that is around the glass transition temperature (between the peak of the tan δ and the inflection of the E' before the final plateau).

This kind of approach could be easily implemented, for example, by tire makers capable of predicting the glass transition temperature T_g by controlling the components such as polymers and resins through equations like the Fox equation, which is a useful tool for calculating the overall T_g starting from mixed components with different T_g values [51].

In the following, for each zone, a range of 10^2 rad/s of frequency has been selected (these ranges could be also expanded), and a 4-elements NLGFMW has been employed. It is worth highlighting that the characterization up to the second plateau was available only for compounds A, B, C, and D, while for the other materials, the available data stopped shortly after the peak of the tan δ. For this reason, for the first mentioned materials, the 3 zones described previously were identified and the results of the model were compared with the experimental data, while for the remaining ones, only data corresponding to the first plateau and the tan δ peak were considered (more strict 2 zones), still giving satisfactory results when compared with available data.

The results for four materials are visible in Fig. 12, while the MAPE errors between the predicted model and the experimental data are listed in Table 5 for all ten materials.

The outcomes are very promising, with an error always below 10% excluded for the MAPE of the tan δ for slab D, for which it is important to remember that only two zones were selected to calibrate the model. Hence, with only three zones that cover a range of 20–30% of the total experimental data, it is possible to achieve reliable results that allow evaluating the viscoelastic properties in a much wider frequency range.

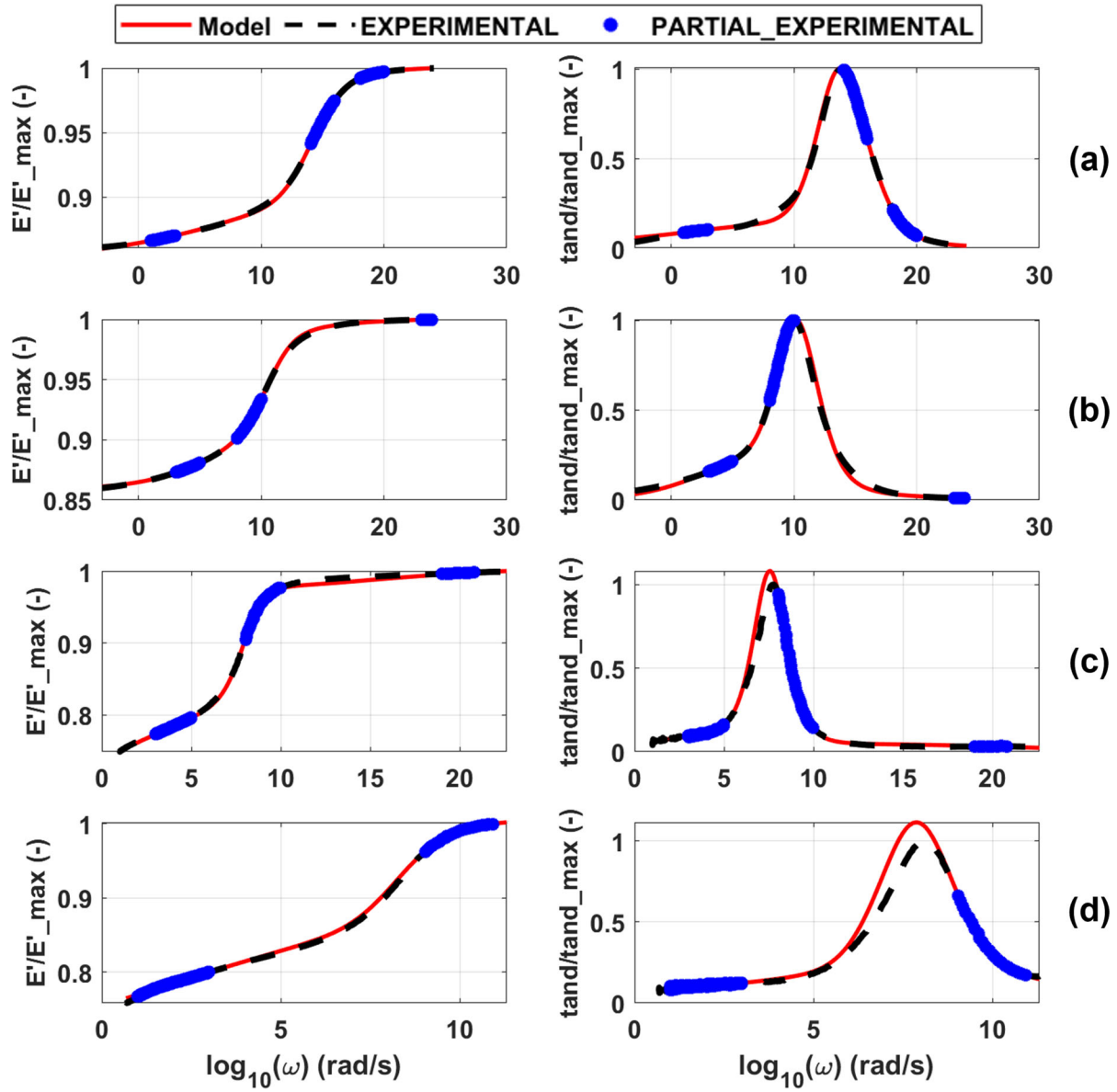

Fig. 12 4-elements NLGFMW model response in terms of E' and tan δ calibrated with limited experimental data for Compound A (**a**), Compound B (**b**), Compound D (**c**), Compound E (**d**)

It is worth observing that each zone is necessary to set appropriate parameters of the formulation of K_0: zone 1 and zone 3 determine the parameters of f_1 of the Eq. (25) and the asymmetry parameter t, as it provides information on the frequency ranges far from the glass transition region; while the zone 2 as part of the transition zone is necessary for the identification of the parameters of f_2 of the Eq. (25). In the case where, as for Compound E in Fig. 12, the information relating to the 3rd zone is missing, the algorithm adapts itself by using only the data available.

This is a valuable achievement since it means that it is not always necessary to cover an extensive range of frequencies when testing a material, but by appropriately choosing the most relevant areas, it is possible to significantly reduce the number of experiments to be carried out by limiting only at specific temperatures and frequencies. This advantage has a significantly pos-

Table 5 MAPE metrics for a 4-elements NLGFMW model calibrated on partial experimental data

	4-elements NLGFMW	
Material	MAPE E' (%)	MAPE tan δ (%)
Compound A	1.198	7.109
Compound B	1.678	9.727
Compound C	1.931	9.646
Compound D	2.892	6.966
Compound E	3.938	6.469
Compound F	2.494	5.662
Slab A	8.468	4.364
Slab B	2.581	3.718
Slab C	2.665	8.028
Slab D	6.896	15.003

itive impact on the employable resources, allowing to minimize the time and costs in the testing phase.

Finally, it is noteworthy that the nonlinear 4-elements model has been chosen to test the capacity to reproduce the material behavior from a limited amount of data, but also in this case the logic scheme presented in Fig. 11 can be applied.

5 Conclusion

The study presented an innovative approach to modeling the mechanical behavior of viscoelastic materials, introducing a nonlinear dependence of stiffness on frequency. Based on the well-established pole-zero formulation for the GFMW, a new formulation has been proposed and mathematically validated to better replicate the dynamic moduli trend for materials with marked nonlinear behavior.

It has been shown that the addition of a nonlinear isolated spring in the model has effects on the formulation of the storage modulus and not the loss factor, consistently with what could be physically expected since that element schematizes a stiffness and not a dampening.

By exploiting the advantages of the pole-zero identification procedure, which allows to overcome computational and convergence problems starting from specific boundary and initials conditions, the optimal multi-objective optimization logic was identified, relying on the MAPE metrics. With these assumptions, the new nonlinear model was implemented and validated on 10 different materials with very diverse mechanical behavior, previously characterized with the DMA technique.

The NLGFMW model has proven to be valid in identifying the viscoelastic properties with even just 3 fractional elements, with errors comparable to those obtained with 5 elements, and with shorter computation times.

Furthermore, the novel nonlinear model has been compared to the previous GFMW, setting a comparable number of parameters, to quantify the improvements obtained. For 7 out of 10 materials, the nonlinear model performed wide better than the linear one, always falling below 7% of error. The only case in which the results were comparable was on 3 compounds with marked transition zones, for which the addition of the non-linear spring is superfluous. These outcomes led to establishing a general approach based on a 17-parameters nonlinear model, with the chance of choosing a constant stiffness or a frequency-dependent one according to the need. Furthermore, the possibility of further reducing the number of parameters is explored, once the type of model best suited to the material under investigation has been established.

Overall, therefore, the new modeling proved to be very efficient in reproducing the behavior of even very different rubber materials, showing greater versatility compared to the classic fractional model, while still maintaining complete physical coherence.

Finally, the validity and stability of the model were investigated even in the case of a small number of experimental data available, to understand the minimum number of tests necessary to be able to reproduce the mechanical characteristics over an extended frequency range. Adopting data coming from the lower and upper frequencies plateau of the storage modulus, and data around the T_g value, the NLGFMW with 4 elements allowed to achieve valuable results, and this could represent an excellent tool for reducing resource usage in the experimental phases.

Author contributions Conceptualization, A.S.; methodology, A.S., R.S.; software, R.M. R.S.; validation, R.M; formal analysis, L.M., R.M.; investigation, R.S.; data curation, R.M. R.S.; writing—original draft preparation, A.S. R.S.; writing—review and editing, L.M. R.M.; supervision, A.S. L.M. All authors have read and agreed to the published version of the manuscript.

Funding Open access funding provided by Università degli Studi di Napoli Federico II within the CRUI-CARE Agreement.

The authors declare that no funds, grants, or other support were received during the preparation of this manuscript.

Data availability The datasets generated and analyzed during the current study are not publicly available but are available from the corresponding author on reasonable request.

Declarations

Conflict of interest The authors have no relevant financial or non-financial interests to disclose.

References

1. Provenzano, P., Lakes, R., Keenan, T., Vanderby, R.: Nonlinear ligament viscoelasticity. Ann. Biomed. Eng. **29**, 908–914 (2001)
2. Garcia-Gonzalez, D., Garzon-Hernandez, S., Arias, A.: A new constitutive model for polymeric matrices: application to biomedical materials. Compos. B Eng. **139**, 117–129 (2018)
3. Hajikarimi, P., Nejad, F.M.: Applications of viscoelasticity: Bituminous materials characterization and modeling. Elsevier, Amsterdam (2021)
4. Khan, A.I., Borowski, E.C., Soliman, E.M., Reda Taha, M.M.: Examining energy dissipation of deployable aerospace composites using matrix viscoelasticity. J. Aerosp. Eng. **30**, 04017040 (2017)
5. Mastroddi, F., Martarelli, F., Eugeni, M., Riso, C.: Time-and frequency-domain linear viscoelastic modeling of highly damped aerospace structures. Mech. Syst. Signal Process. **122**, 42–55 (2019)
6. Nakra, B.: Vibration control in machines and structures using viscoelastic damping. J. Sound Vib. **211**, 449–466 (1998)
7. González-Vega, J., Castillo-López, G., Galindo-Moreno, J.M., Guerrero-Porras, S., García-Sánchez, F.: Experimental viscoelastic properties evaluation, under impact loads and large strain conditions, of coated & uncoated rubber from end-of-life tires. Polym. Test. **107**, 107468 (2022)
8. Nakanishi, R., Matsubara, M., Ishibashi, T., Kawasaki, S., Suzuki, H., Kawabata, H., Kawamura, S., Tajiri, D.: Tire mechanical model for cornering simulation with friction coefficient calculated from viscoelasticity of rubber by multiscale friction theory. Veh. Syst. Dyn. **1**, 1–2 (2023). https://doi.org/10.1080/00423114.2023.2290239
9. Li, Y., Tang, S., Kröger, M., Liu, W.K.: Molecular simulation guided constitutive modeling on finite strain viscoelasticity of elastomers. J. Mech. Phys. Solids **88**, 204–226 (2016)
10. Chevallier, G., Renaud, F., Dion, J.-L., Thouviot, S.: Complex eigenvalue analysis for structures with viscoelastic behavior. In: International design engineering technical conferences and computers and information in engineering conference, vol. 54785, pp. 561–569 (2011)
11. Hinze, M., Schmidt, A., Leine, R.I.: Finite element formulation of fractional constitutive laws using the reformulated infinite state representation. Fractal Fract. **5**, 132 (2021)
12. Bland, D.R.: The theory of linear viscoelasticity. Courier Dover Publications, Mineola (2016)
13. Menard, K.P., Menard, N.: Dynamic mechanical analysis. CRC Press, Boca Raton (2020)
14. Farroni, F., Genovese, A., Maiorano, A., Sakhnevych, A., Timpone, F.: Development of an innovative instrument for non-destructive viscoelasticity characterization: VESevo in Advances in Italian Mechanism Science. In: Proceedings of the 3rd international conference of IFToMM Italy, vol. 3, pp. 804–812 (2021)
15. Shaw, M.T., MacKnight, W.J.: Introduction to polymer viscoelasticity. Wiley, Amsterdam (2018)
16. Mark, J.E., Erman, B., Roland, M.: The science and technology of rubber. Academic press, London (2013)
17. Gutierrez-Lemini, D.: Engineering viscoelasticity. Springer, New York (2014)
18. Bonfanti, A., Kaplan, J.L., Charras, G., Kabla, A.: Fractional viscoelastic models for power-law materials. Soft Matter **16**, 6002–6020 (2020)
19. Koeller, R.C.: Applications of Fractional Calculus to the Theory of Viscoelasticity. J. Appl. Mech. **51**, 299–307 (1984)
20. Gaul, L., Klein, P., Kemple, S.: Damping description involving fractional operators. Mech. Syst. Signal Process. **5**, 81–88 (1991)
21. Lion, A.: On the thermodynamics of fractional damping elements. Contin. Mech. Thermodyn. **9**, 83–96 (1997)
22. Liu, J.G., Xu, M.Y.: Higher-order fractional constitutive equations of viscoelastic materials involving three different parameters and their relaxation and creep functions. Mech. Time-Depend. Mater. **10**, 263–279 (2006)
23. Bhangale, N., Kachhia, K.B., Gómez-Aguilar, J.: Fractional viscoelastic models with Caputo generalized fractional derivative. Math. Methods Appl. Sci. **46**, 7835–7846 (2023)
24. Shitikova, M.: Fractional operator viscoelastic models in dynamic problems of mechanics of solids: a review. Mech. solids **57**, 1–33 (2022)
25. Meral, F., Royston, T., Magin, R.: Fractional calculus in viscoelasticity: an experimental study. Commun. Nonlinear Sci. Numer. Simul. **15**, 939–945 (2010)
26. Wagner, C.E., Barbati, A.C., Engmann, J., Burbidge, A.S., McKinley, G.H.: Quantifying the consistency and rheology of liquid foods using fractional calculus. Food Hydrocoll. **69**, 242–254 (2017)
27. Faber, T., Jaishankar, A., McKinley, G.: Describing the firmness, springiness and rubberiness of food gels using frac-

tional calculus. Part II: Measurements on semi-hard cheese. Food Hydrocoll **62**, 325–339 (2017)
28. Miranda-Valdez, I.Y., Puente-Córdova, J.G., Rentería-Baltiérrez, F.Y., Fliri, L., Hummel, M., Puisto, A., Koivisto, J., Alava, M.J.: Viscoelastic phenomena in methylcellulose aqueous systems: application of fractional calculus. Food Hydrocoll. **147**, 109334 (2024)
29. Wang, P., Yang, S., Liu, Y., Zhao, Y.: Experimental study and fractional derivative model prediction for dynamic viscoelasticity of magnetorheological elastomers. J. Vib. Eng. Technol. **10**, 1865–1881 (2022)
30. Patel, D., Upadhyay, R.V.: Fractional Maxwell viscoelastic model to explain dynamic magneto-viscoelastic properties of an isotropic magnetorheological elastomer containing flake-shaped magnetic particles. Soft Mater. **21**, 1–12 (2023)
31. Zhou, S., Cao, J., Chen, Y.: Genetic algorithm-based identification of fractional-order systems. Entropy **15**, 1624–1642 (2013)
32. Arikoglu, A.: A new fractional derivative model for linearly viscoelastic materials and parameter identification via genetic algorithms. Rheol. Acta **53**, 219–233 (2014)
33. De Espındola, J.J., da Silva Neto, J.M., Lopes, E.M.: A generalised fractional derivative approach to viscoelastic material properties measurement. Appl. Math. Comput. **164**, 493–506 (2005)
34. Sasso, M., Palmieri, G., Amodio, D.: Application of fractional derivative models in linear viscoelastic problems. Mech. Time-Depend. Mater. **15**, 367–387 (2011)
35. Yuan, L., Agrawal, O.P.: A numerical scheme for dynamic systems containing fractional derivatives. J. Vib. Acoust. **124**, 321–324 (2002)
36. Lewandowski, R., Chorążyczewski, B.: Identification of the parameters of the Kelvin-Voigt and the Maxwell fractional models, used to modeling of viscoelastic dampers. Comput. struct. **88**, 1–17 (2010)
37. Renaud, F., Dion, J.-L., Chevallier, G., Tawfiq, I., Lemaire, R.: A new identification method of viscoelastic behavior: application to the generalized Maxwell model. Mech. Syst. Signal Process. **25**, 991–1010 (2011)
38. Genovese, A., Carputo, F., Maiorano, A., Timpone, F., Farroni, F., Sakhnevych, A.: Study on the generalized formulations with the aim to reproduce the viscoelastic dynamic behavior of polymers. Appl. Sci. **10**, 2321 (2020)
39. Heymans, N.: Fractional calculus description of non-linear viscoelastic behaviour of polymers. Nonlinear Dyn. **38**, 221–231 (2004)
40. Monsia, M.D.: A simplified nonlinear generalized Maxwell model for predicting the time dependent behavior of viscoelastic materials. World J. Mech. (2011). https://doi.org/10.4236/wjm.2011.13021
41. Jrad, H., Dion, J.L., Renaud, F., Tawfiq, I., Haddar, M.: Experimental characterization, modeling and parametric identification of the non linear dynamic behavior of viscoelastic components. Eur. J. Mech. A/Solids **42**, 176–187 (2013)
42. Dorleans, V., Delille, R., Notta-Cuvier, D., Lauro, F., Michau, É.: Time-temperature superposition in viscoelasticity and viscoplasticity for thermoplastics. Polym. Test. **101**, 107287 (2021)
43. Ferry, J.D.: Viscoelastic properties of polymers. Wiley, Amsterdam (1980)
44. Palmeri, A., Ricciardelli, F., De Luca, A., Muscolino, G.: State space formulation for linear viscoelastic dynamic systems with memory. J. Eng. Mech. **129**, 715–724 (2003)
45. Dion, J.-L.: Modélisation et identification du comportement dynamique des liaisons hydro-élastiques Diss. Châtenay-Malabry, Ecole centrale de Paris (1995)
46. Dion, J., Vialard, S.: Identification or rubber shock absorber mounts. Mécanique Ind. et matériaux **50**, 232–237 (1997)
47. Guo, K., Zhang, L.: Multi-objective optimization for improved project management: current status and future directions. Autom. Constr. **139**, 104256 (2022)
48. Tan, K.C., Lee, T.H., Khor, E.F.: Evolutionary algorithms for multi-objective optimization: performance assessments and comparisons. Artif. Intell. Rev. **17**, 251–290 (2002)
49. Deb, K., Pratap, A., Agarwal, S., Meyarivan, T.: A fast and elitist multiobjective genetic algorithm: NSGA-II. IEEE Trans. Evol. Comput. **6**, 182–197 (2002)
50. Ma, H., Zhang, Y., Sun, S., Liu, T., Shan, Y.: A comprehensive survey on NSGA-II for multi-objective optimization and applications. Artif. Intell. Rev. **56**, 15217–15270 (2023)
51. Vleugels, N., Pille-Wolf, W., Dierkes, W.K., Noordermeer, J.W.: Influence of oligomeric resins on traction and rolling resistance of silica tire treads. In: 184th Technical Meeting ACS Rubber Division, pp. 1–24 (2013)
52. Anilkumar, P., Manjunatha, L., Venkategowda, T.: Dynamic mechanical analysis of graphene and nano silica reinforced hybrid epoxy composites under dual cantilever mode. Mater. Today Proc. **54**, 402–408 (2022)
53. Chowdhury, S., Fabiyi, J., Frazier, C.E.: Advancing the dynamic mechanical analysis of biomass: comparison of tensile-torsion and compressive-torsion wood DMA. Holzforschung (2010). https://doi.org/10.1515/hf.2010.123
54. fmincon - Constrained nonlinear optimization function. https://it.mathworks.com/help/optim/ug/fmincon.html. Accessed 31 July 2024